Eletrônica de Potência
Open Journal of Power Electronics

Received July 31, 2024; accepted November 30, 2024; Date of publication December 17, 2024.
The review of this paper was arranged by Associate Editor Roberto F. Coelho and Editor-in-Chief Heverton A. Pereira.

Digital Object Identifier http://doi.org/10.18618/REP.e202458

OSV-MPC for Harmonic and Zero-Sequence Compensation in Four-Wire Off-Grid Microgeneration Systems Based on SEIG

Carlos A. Souza[1], Gabriel M. Cocco[1,2], Robinson F. de Camargo[1], Fábio E. Bisogno[3] and Martin Wolter[2]

[1]Federal University of Santa Maria, Power Electronics and Control Research Group, Santa Maria - RS, Brazil
[2]Otto-von-Guericke University Magdeburg, Institute of Electric Power Systems, Magdeburg - ST, Germany
[3]Koblenz University of Applied Sciences, Koblenz - RP, Germany

e-mail: souza.engeeletrica@gmail.com, maiercocco@gmail.com, robinson.camargo@gmail.com, fbisogno@gmail.com, and martin.wolter@ovgu.de

ABSTRACT This paper proposes a finite control set model predictive control (FCS-MPC) strategy to address voltage regulation in isolated four-wire microgeneration systems based on self-excited induction generators. The FCS-MPC approach enables a simpler and more functional imbalance controller design. The controller determines the optimal switching vector through a cost function that employs a weighting factor for the different control variables. It effectively tracks distorted current references and prevents voltage imbalance, even in a system without frequency regulation. The employed inverter is a four-leg voltage source inverter, also known as a distribution static synchronous compensator, which provides the necessary reactive power and compensates for harmonic content along with the zero-sequence component, ensuring balanced three-phase voltages at the point of common coupling, even with unbalanced loads. The proposed control leverages the instantaneous power theory for synchronization, thereby replacing methods such as the phase-locked loop. Experimental results validate the effectiveness of the proposed control approach and assess the performance of the system in accordance with power quality standards.

KEYWORDS Off-Grid Microgeneration, Induction Generator, Four-Wire System, Model Predictive Control, Zero-Sequence Voltage, Harmonic Current Compensation.

I. INTRODUCTION

The integration of renewable energy sources into distributed generation systems, particularly in microgeneration systems, offers a promising avenue for reducing costs associated with conventional transmission and distribution infrastructure. Self-Excited Induction Generators (SEIGs) emerge as key components in these systems, drawing from water, wind, or biomass resources [1]–[3]. In this sense, SEIGs play a crucial role in voltage regulation, dependent on the balance between reactive and active power within the AC bus. Nevertheless, they are susceptible to load variations, leading to changes in machine slip and consequent variations in reactive power and synchronous speed. To ensure voltage regulation at the point of common coupling (PCC), various topologies for reactive power compensation have been proposed for SEIGs [4], [5].

Among these solutions, the four-leg inverter, also known in this application as a Distribution Static Synchronous Compensator (DSTATCOM), stands out for its effectiveness in voltage regulation and compensation of reactive power and harmonic components. This type of inverter is adept at providing balanced voltages for a wide range of load configurations, including linear, nonlinear, balanced, and unbalanced loads, with the midpoint of the fourth leg serving as the neutral point for connected loads [6]–[8]. The system studied in this paper is represented in Figure 1. The Model Predictive Control (MPC) is considered an algorithm that utilizes the system model to predict its future behavior and selects the most suitable control action based on an optimization criterion [9]. The predictive controller is widely applied in four-leg converters due to its fast dynamic response, surpassing classical controllers, both proportional-integral (PI) and proportional-resonant (PR) controllers [10]–[16]. The main advantages of using MPC are its ability to track alternating signals, regardless of the designed frequency, handle saturation, switching frequency, and power losses,as well as allow for the inclusion of constraints directly in the optimization process, which enhances control flexibility and robustness [10], [17].

MPC for power electronics can be categorized into two primary groups: continuous control set (CCS-MPC) and finite control set (FCS-MPC). CCS-MPC boasts a significant advantage in its utilization of a continuous control signal coupled with a pulse-width modulator, ensuring a consistent switching frequency. This design simplifies the development of power filters [18]. However, it comes with a trade-off, reducing the control speed by not ensuring the maximum

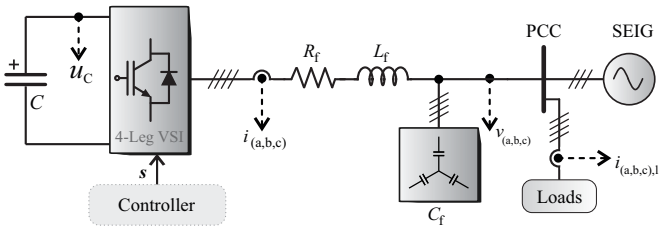

FIGURE 1. Diagram of the microgeneration system.

possible control action. Additionally, this method excels when dealing with unconstrained optimization problems, allowing for offline analytical solutions. Nevertheless, it can become mathematically complex, particularly when introducing constraints. On the other hand, among the various approaches available, FCS-MPC leverages the inherent discrete characteristics of power converters [9]. Because these converters possess a finite number of switching states, the optimization challenge revolves around predicting system behavior within those available switching states over a short-term horizon. In this paper, the focus is on the proposed optimal switching vector MPC (OSV-MPC) approach. The OSV-MPC, a subtype of FCS-MPC, is the most popular MPC strategy for power electronics, often referred to as FCS-MPC in the literature [17]. A limitation of OSV-MPC is that, in the absence of a modulator, the switching frequency is not enforced to remain constant. OSV-MPC considers only the possible switching states as the control set, applying one of them during the entire sampling period, simplifying the optimization problem to an enumerated search algorithm, resulting in a simpler and more intuitive solution [10], [19].

This paper proposes the use of OSV-MPC for inverter currents and also for the neutral point voltage at the PCC, which is used to compensate for imbalances caused by unbalanced loads connected to the system. To meet the requirements of voltage regulation, harmonic compensation, and imbalances in the proposed four-wire system, the use of OSV-MPC is essential, with its fast dynamic response, intuitive formulation, and easy consideration of nonlinearities and constraints in the control of variables of different scales, such as current and voltage, in a single control loop. Some challenges of OSV-MPC are encountered in the design of the cost function, but these can be addressed by including a weighting factor (λ), which aids in the operational performance of the controlled variables [10]. This strategy was not found in the literature for this isolated four-wire microgeneration system based on SEIG and VSI, providing a solution to the control tracking problems indicated in [6], [12], [16].

Experimental results are presented to validate the performance of the proposed control strategy for the system in terms of power quality, according to the IEEE 519-2014 standard for total harmonic distortion (THD) and the IEEE 1159-2009 standard for voltage imbalances. The main contributions of this paper can be summarized as follows:

- Application of OSV-MPC in a four-leg VSI connected to an isolated microgeneration system based on SEIG
- Proposal and implementation of a specific cost function in OSV-MPC strategy that considers voltage imbalance regulation, harmonic tracking, and zero sequence compensation for the off-grid microgeneration system
- The use of instantaneous power theory for system synchronization, based on three-phase voltages, reducing computational burden, enabling an increase in the sampling frequency, differing from [16]

II. SYSTEM DESCRIPTION AND MODELING

From the system diagram (see Figure 1), the inverter is connected to PCC. Each of the sixteen switching states of the four-leg VSI corresponds to one output voltage vector in abc coordinates. The Clarke power invariant transformation can represent these output voltage vectors in the $\alpha\beta0$ frame. The dynamics of the output currents in $\alpha\beta0$ can be written as a discrete-time state-space model for a sampling period T_s, and a forward Euler approximation can be used to predict the future value of the variables by:

$$\hat{\boldsymbol{i}}_{\alpha\beta0,k+1} = (\boldsymbol{I} + \boldsymbol{A}T_s)\,\boldsymbol{i}_{\alpha\beta0,k} + \boldsymbol{B}T_s\left(\boldsymbol{u}_{\alpha\beta0,k} - \boldsymbol{v}_{\alpha\beta0,k}\right), \quad (1)$$

$$\hat{v}_{0,k+1} = v_{0,k} - \frac{T_s}{C_f} i_{0,l,k} + \frac{T_s}{C_f} i_{0,k}, \quad (2)$$

where $\boldsymbol{v}_{\alpha\beta0} = [v_\alpha \;\; v_\beta \;\; v_0]^\top$ are PCC voltages, and $\boldsymbol{u}_{\alpha\beta0}$ are the inverter output voltages. The state-space matrices follow the well-known model presented in [16]:

$$\dot{\boldsymbol{i}}_{\alpha\beta0}(t) = \boldsymbol{A}\boldsymbol{i}_{\alpha\beta0}(t) + \boldsymbol{B}\left(\boldsymbol{u}_{\alpha\beta0}(t) - \boldsymbol{v}_{\alpha\beta0}(t)\right), \quad (3)$$

where

$$\boldsymbol{A} = \begin{bmatrix} \frac{-R_f}{L_f} & 0 & 0 \\ 0 & \frac{-R_f}{L_f} & 0 \\ 0 & 0 & \frac{-R_f}{L_f} \end{bmatrix} \boldsymbol{B} = \begin{bmatrix} \frac{1}{L_f} & 0 & 0 \\ 0 & \frac{1}{L_f} & 0 \\ 0 & 0 & \frac{1}{4L_f} \end{bmatrix}. \quad (4)$$

Moreover, a step ahead can be included to compensate for the implementation time of the microprocessor, according to [20]. In addition, as the frequency of $\boldsymbol{v}_{\alpha\beta0}$ and $\boldsymbol{i}_{\alpha\beta0}$ are much smaller than the sampling frequency, it can be assumed that $\boldsymbol{v}^*_{\alpha\beta0,k} \approx \boldsymbol{v}^*_{\alpha\beta0,k+1}$ and $\boldsymbol{i}^*_{\alpha\beta0,k} \approx \boldsymbol{i}^*_{\alpha\beta0,k+1}$.

Table 1 shows the sixteen switching states of the power converter. Each state corresponds to one output voltage vector represented in the $\alpha\beta0$ frame.

III. CONTROLLERS

The applied control strategy is depicted in Figure 2. The proposed scheme presents an OSV-MPC combined with a linear Proportional-Integral (PI) control. The system inputs include phase voltages, inverter currents, load currents, and the DC bus voltage. Clarke transformation is applied to the voltages and currents to decouple system variables, aiding in the analysis of harmonic and zero sequence components.

Two PI controllers are used: one for controlling the DC bus voltage and the other for the AC voltages at the PCC. The OSV-MPC employs predictive modeling to calculate the optimal switching vector, minimizing a cost function

TABLE 1. Switching States and Output Voltages

Index	Switching state				Output voltage		
j	S_1	S_2	S_3	S_4	u_α	u_β	u_0
1	0	0	0	0	0	0	0
2	0	0	0	1	0	0	$-\sqrt{3}u_C$
3	0	0	1	0	$-\sqrt{\frac{2}{3}}u_C/2$	$-u_C/\sqrt{2}$	$u_C/\sqrt{3}$
4	0	0	1	1	$-\sqrt{\frac{2}{3}}u_C/2$	$-u_C/\sqrt{2}$	$-2u_C/\sqrt{3}$
5	0	1	0	0	$-\sqrt{\frac{2}{3}}u_C/2$	$u_C/\sqrt{2}$	$u_C/\sqrt{3}$
6	0	1	0	1	$-\sqrt{\frac{2}{3}}u_C/2$	$u_C/\sqrt{2}$	$-2u_C/\sqrt{3}$
7	0	1	1	0	$-\sqrt{\frac{2}{3}}u_C$	0	$2u_C/\sqrt{3}$
8	0	1	1	1	$-\sqrt{\frac{2}{3}}u_C$	0	$-u_C/\sqrt{3}$
9	1	0	0	0	$\sqrt{\frac{2}{3}}u_C$	0	$u_C/\sqrt{3}$
10	1	0	0	1	$\sqrt{\frac{2}{3}}u_C$	0	$-2u_C/\sqrt{3}$
11	1	0	1	0	$\sqrt{\frac{2}{3}}u_C/2$	$-u_C/\sqrt{2}$	$2u_C/\sqrt{3}$
12	1	0	1	1	$\sqrt{\frac{2}{3}}u_C/2$	$-u_C/\sqrt{2}$	$-u_C/\sqrt{3}$
13	1	1	0	0	$\sqrt{\frac{2}{3}}u_C/2$	$u_C/\sqrt{2}$	$2u_C/\sqrt{3}$
14	1	1	0	1	$\sqrt{\frac{2}{3}}u_C/2$	$u_C/\sqrt{2}$	$-u_C/\sqrt{3}$
15	1	1	1	0	0	0	$\sqrt{3}u_C$
16	1	1	1	1	0	0	0

that considers control variables such as inverter currents and the zero-sequence voltage, related to the fourth or neutral wire. Measurements are sampled at each interval T_s, corresponding to the current and voltage data in discrete time, for each sampling instant k. The instantaneous power theory is used for synchronization by relating inverter active (p) and reactive (q) power with the three-phase voltages at the PCC. Finally, the controller generates the switching state as a control action $\boldsymbol{s}$, which acts directly on the power switches, in this case, the IGBTs.

The reference currents are generated in the stationary $\alpha\beta0$ reference frame. Employing the p-q theory and the power invariant Clarke transformation, these quantities are found based on the control action of the PCC voltage and DC-bus voltage controllers. The other part of the current references is obtained directly by the load currents:

$$\begin{bmatrix} i_\alpha^* \\ i_\beta^* \end{bmatrix} = \begin{bmatrix} i_{\alpha,1} \\ i_{\beta,1} \end{bmatrix} + \frac{1}{v_\alpha^2 + v_\beta^2} \begin{bmatrix} v_\alpha & v_\beta \\ v_\beta & -v_\alpha \end{bmatrix} \begin{bmatrix} p^* \\ q^* \end{bmatrix}. \tag{5}$$

The zero-sequence current compensation is performed by measuring the load current. Then the inverter supplies the required current through the neutral conductor [21]. This compensation can be done using the MPC, directly considering the load current $i_{0,1}$. Thus, the control strategy tracks the amount of current to be injected through neutral,

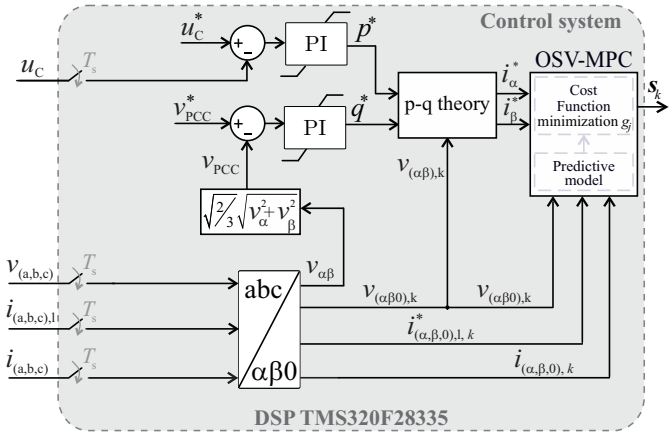

FIGURE 2. Block diagram of the multi-loop control system.

which is drawn by the load. To control the 0 axis, the predictive controller input requires the load current $i_{0,1}$, that is,

$$i_0^* = i_{0,1}. \tag{6}$$

The reference currents found by (5) and (6) are evaluated using a saturation boundary, considering the inverter current ratings. These variables, along with other measurements, are utilized in the OSV-MPC technique, presented in the following subsections.

A. Outer control loops

The prediction model is fed by model states $\boldsymbol{i}_{\alpha\beta0}$ and $\boldsymbol{v}_{\alpha\beta0}$. In addition, the outer loop controllers determine the current references related to the regulation of PCC voltages and also to the DC bus voltage. These values are transformed to $\alpha\beta0$ currents for the cost function of the predictive controller, responsible for controlling the currents processed by the inverter, also using the desired compensation of the load currents $i_{\alpha,1}$, $i_{\beta,1}$, and $i_{0,1}$. Finally, these generate the switching state as a control action. If there are imbalances between the load currents an alternating component appears in the current $i_{0,1}$, causing an imbalance in PCC voltages [12], [16], and also generating an alternating component in the voltage v_0. The control of these voltage loops depends exclusively on the feedback of the system voltages, making it necessary to measure the PCC phase voltages and the DC bus voltage of the DSTATCOM. Thereupon, discrete-time proportional-integral controllers can be used to provide control action in the outer loops as

$$\begin{cases} \dot{\boldsymbol{x}}_{\mathrm{I},k} = \boldsymbol{e}_{\mathrm{pq},k} \\ \boldsymbol{y}_k^* = \boldsymbol{k}_\mathrm{I}\boldsymbol{x}_{\mathrm{I},k} + \boldsymbol{k}_\mathrm{P}\boldsymbol{e}_{\mathrm{pq},k}, \end{cases} \tag{7}$$

with

$$\boldsymbol{x}_{\mathrm{I},k+1} = \boldsymbol{x}_{\mathrm{I},k} + T_\mathrm{s}\boldsymbol{e}_{\mathrm{pq},k}, \tag{8}$$

where $\boldsymbol{x}_{\mathrm{I},k} = [x_{\mathrm{I,p},k} \quad x_{\mathrm{I,q},k}]^\top$ are the accumulation variables for the error integration, $\boldsymbol{y}_k^* = [p_k^* \quad q_k^*]^\top$, $\boldsymbol{k}_\mathrm{P}$ and $\boldsymbol{k}_\mathrm{I}$ are respectively the proportional and integral gain of the PI

controller, arranged as column vectors as $\boldsymbol{k}_{\mathrm{P}} = [K_{\mathrm{P,p}} \quad K_{\mathrm{P,q}}]^{\top}$ and $\boldsymbol{k}_{\mathrm{I}} = [K_{\mathrm{I,p}} \quad K_{\mathrm{I,q}}]^{\top}$, and $\boldsymbol{e}_{\mathrm{pq}}$ represents the error:

$$\boldsymbol{e}_{\mathrm{pq},k} = \left[u^{*}_{\mathrm{C},k} - u_{\mathrm{C},k} \quad v^{*}_{\mathrm{PCC},k} - v_{\mathrm{PCC},k}\right]^{\top}. \tag{9}$$

This implementation is particularly suitable for applying the conditional integration anti-windup technique. For the design of the PI controllers, the method described in 16 was adopted, considering an adequate gain margin, and a phase margin of at least 45 degrees to prevent oscillations or instability. The proportional and integral gains are tuned according to the stability criteria to achieve low frequency, avoiding disturbances caused by interaction with the switching frequency and the variables controlled by the MPC.

B. Model predictive control description

MPC aims to predict the future behavior of the variables. Therefore, an appropriate control action must be defined to bring these variables close to the reference values. In this regard, the measured variables $\boldsymbol{x}_k$ are used to compensate for control implementation time through a predictive function f_{p} that relates the sampled values and the present state of the inverter $\boldsymbol{s}_k$, for getting $\hat{\boldsymbol{x}}_{k+1}$. Thus, to predict future values of the system, the predictive function is used to obtain $\hat{\boldsymbol{x}}_{k+2,j}$, which represents the prediction to $\hat{\boldsymbol{x}}_{k+2}$ for the inverter possible states $\boldsymbol{s}_j$. Subsequently, a cost function f_{g} can be defined to find the optimal state between the sixteen resulting values, for this, the cost function will relate the references of the variables and their predicted values. Therefore, the control action $\boldsymbol{s}_{k+1}$ that brings $\boldsymbol{x}$ as close as possible to the desired reference $\boldsymbol{x}^{*}$ should minimize the cost function according to:

$$g_j = f_{\mathrm{g}}\left\{\boldsymbol{x}^{*}, \hat{\boldsymbol{x}}_{k+2,j}\right\}, \tag{10}$$

where

$$\hat{\boldsymbol{x}}_{j,k+2} = f_{\mathrm{p}}\left\{\hat{\boldsymbol{x}}_{k+2}, \boldsymbol{s}_j\right\}, \ \forall j \in \{1,2,...,16\}, \tag{11}$$

where f_{p} is the discrete model for the predicted variables $\boldsymbol{i}_{\alpha\beta 0}$ and v_0. There are several ways to define a cost function depending on the nature of the different terms involved in the problem formulation [17]. The proposed cost function is defined as:

$$\begin{aligned} g_j = &\left(i^{*}_{\alpha} - \hat{i}_{\alpha,k+2,j}\right)^2 + \left(i^{*}_{\beta} - \hat{i}_{\beta,k+2,j}\right)^2 + \left(i_{0,\mathrm{l}} - \hat{i}_{0,k+2,j}\right)^2 \\ &+ \lambda \hat{v}^2_{0,k+2,j}, \end{aligned} \tag{12}$$

where λ is a proper weight factor and the zero axis voltage reference is set to zero.

Stability analysis in FCS-MPC presents a challenge and is often approached with heuristic methods. Some studies adopt recursive approaches to support this analysis. For instance, [22] applies FCS-MPC with the Lyapunov function for current control in VSI, ensuring stability and convergence of current errors. Similarly, [23], [24] utilize the Lyapunov function to guarantee closed-loop stability.

C. Cost function with weighting factor

One of the main advantages of OSV-MPC is its flexibility in the cost function, allowing the inclusion of additional terms that may represent a prediction for another system variable, a constraint, or a requirement of the system. This flexibility enables the achievement of various control objectives, such as improving system performance and power quality [25].

This approach acknowledges that different variables in a cost function may have distinct physical natures (current, voltage, reactive power, switching losses, torque, flux, etc.), which can lead to challenges such as variable coupling or overestimation of the importance of one term compared to others. To address this, weighting coefficients or factors (λ), are commonly used, aiding in balancing each variable in the cost function [19]. Depending on the nature of the terms in the cost function, they can be grouped into distinct categories, which facilitates the selection of weighting factors.

Higher values of these factors increase the priority assigned to the corresponding term, causing switching penalties on the tracking error [26], [27]. Properly adjusting the weighting factors is crucial in the design of an OSV-MPC-based controller, as different operational conditions require different priorities. Currently, the weighting factors are determined empirically, as there is no analytical or numerical method for obtaining an optimal solution for these coefficients in the literature [25]. Therefore, a practical approach is to select an operating condition and implement different weighting factors, then analyze the resulting behaviors to determine their most appropriate performance

D. MPC algorithm

The MPC Algorithm 1 is shown below in pseudocode form. To solve the optimization problem, it uses a *for loop* that solves the prediction equations for each voltage vector.

Algorithm 1: Proposed MPC algorithm

```
Sampling i_αβ0,k, v_αβ0,k, i_αβ0,l,k, u_C,k;
î_αβ0,k+1, v̂_0,k+1, ← f_p {x_k, s_k};
g_min ← ∞;
for each j from 1 to 16 do
    î_αβ0,k+2,j ← f_p {î_αβ0,k+1, s_j, v_αβ0,k};
    v̂_0,k+2,j ← f_p {v̂_0,k+1, î_0,k+1, i_0,l,k};
    g_j = f_g {x*_k+2, x̂_k+2,j};
    if g_j < j_min then
        j_min ← g_j;
        j_opt ← j;
    end
end
s_k+1 ← s_j_opt;
```

The algorithm starts by sampling the measurement of the system states and predicting currents and voltages for the instant $k+1$, using the prediction function f_{p}, which relies on the current states $\boldsymbol{x}_k$ and the applied switching state

s_k. This enables the prediction of $\hat{\boldsymbol{i}}_{\alpha\beta0,k+1}$ and $\hat{v}_{0,k+1}$, and compensates for the delay caused by the implementation in the microprocessor, while the next control action is being calculated. The cost function $g_{\min}$, initialized with a very high value, is designed to be minimized by comparing the reference values with the predicted responses. The algorithm then iterates over 16 combinations of switching states. For each voltage vector, the variables $\hat{\boldsymbol{i}}_{\alpha\beta0,k+2,j}$ and $\hat{v}_{0,k+2}$ are predicted. The optimal vector is selected by determining which g_j is lower than the current $g_{\min}$, updating $g_{\min}$ and storing the index j_{opt}. Finally, the optimal vector j_{opt} is directly applied to control the power switches.

IV. EXPERIMENTAL RESULTS

In this section, the validation of the proposed OSV-MPC design is presented through experimental results obtained from the test bench illustrated in Figure 3.

FIGURE 3. Experimental setup.

The results are based on the SEIG and VSI parameters described in Table 2. The first test investigates the effect of selecting an appropriate weighting factor value in the cost function, which is used to achieve optimal control performance based on the operational conditions for load connection. The second test involves observing the connection of a 4.2 kVA three-phase nonlinear load to the system. This load is a three-phase rectifier that causes voltage sags and a high harmonic spectrum in the system voltage, adversely affecting performance concerning power quality standards. The third condition involves the connection of three separate 1 kVA single-phase loads, connected respectively to phases a, b, and c, consisting of three single-phase rectifiers. These loads not only cause voltage harmonics but also generate imbalances that reflect on the neutral conductor of the system. The verification of the experimental results analyzes compliance with power quality standards, according to IEEE 519 for voltage THD and IEEE 1159-2009 for voltage imbalance.

The control algorithm is implemented on a TMS320F28335 DSP with a sampling period of T_s = 25 µs, enhancing control performance compared to the sampling period of T_s = 40 µs used in the study [8]. The algorithm execution time for each task in the DSP is presented in Table 3.

TABLE 2. System Parameters

Description	Value
SEIG	
Nominal power	P_n = 3.7 kW (5 cv)
Line voltage (RMS)	V_s = 380 V
Nominal rotor speed	n = 1730 rpm
Frequency	f = 60 Hz
Power factor	FP = 0.81
Excitation capacitor	C_f = 40 µF
Thévenin equivalent	L_g= 5 mH, R_g= 0.2 Ω
Inverter	
Sampling period	T_s = 25 µs
DC bus voltage	u_C = 650 V
DC-link capacitor	C = 4.700 µF
Output filter	L_f= 3.2 mH, R_f= 0.26 Ω
PI Controllers	**Gains**
DC bus voltage u_C	$K_{P,p} = 40, K_{I,p} = 250$
PCC voltage v_{PCC}	$K_{P,q} = 5, K_{I,q} = 1000$

TABLE 3. Computational Time

Task	Total execution time
OSV-MPC algorithm from [8]	27.5 µs
OSV-MPC algorithm from this paper	22.3 µs

A. Weighting factor selection

For the application and experimental test conditions, it is necessary to define, through an operating point, an appropriate value for the weighting factor within the cost function. Careful balancing is crucial to avoid compromising the stability and performance of the system. To this end, an operating condition was selected to analyze the variation of the weight factor.

Figure 4 shows the voltage harmonic spectrum of the system with the weight factor variation in the presence of a 4.2 kVA three-phase nonlinear load.

The weighting factor with the lowest voltage THD for this operating condition is λ = 0.5, which is considered throughout the results of this paper due to its better performance.

B. Reference tracking of system voltages

The response of the OSV-MPC control can be assessed by evaluating the performance of the applied controllers under reference signal variations for the variables of interest. These variations allow us to observe the ability of the controllers to converge to imposed changes, demonstrating their adequate response.

Figures 5(a), 5(b), and 5(c) respectively, present the transient response of the voltage control loops, the inverter DC bus, the PCC voltages on v_{PCC} and the PCC voltages on axis 0. In this case, there is a variation in the voltage

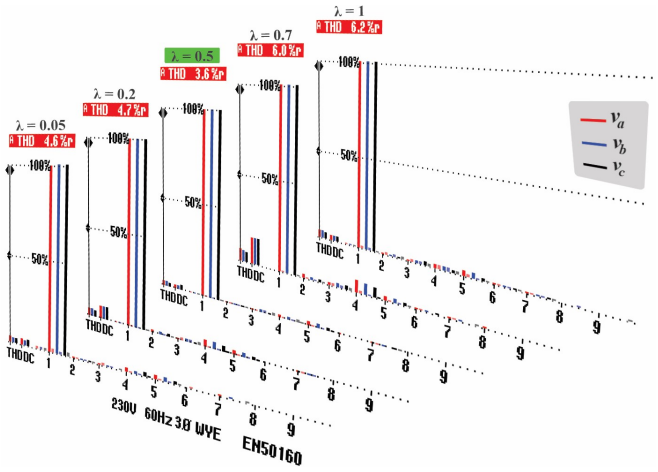

FIGURE 4. Comparison of voltage THD for different weighting factors, when connecting a 4.2 kVA three-phase nonlinear balanced load.

reference signal u_C^* from 650 V to 600 V, as well as in v_{PCC}^* from 311 V to 261 V. Finally, for v_0^*, the control of v_0 is initially inhibited, and then there is a variation in the voltage reference signal v_0^* from 0 V to 30 V, compensating for variations on axis 0 from no load to compensation on.

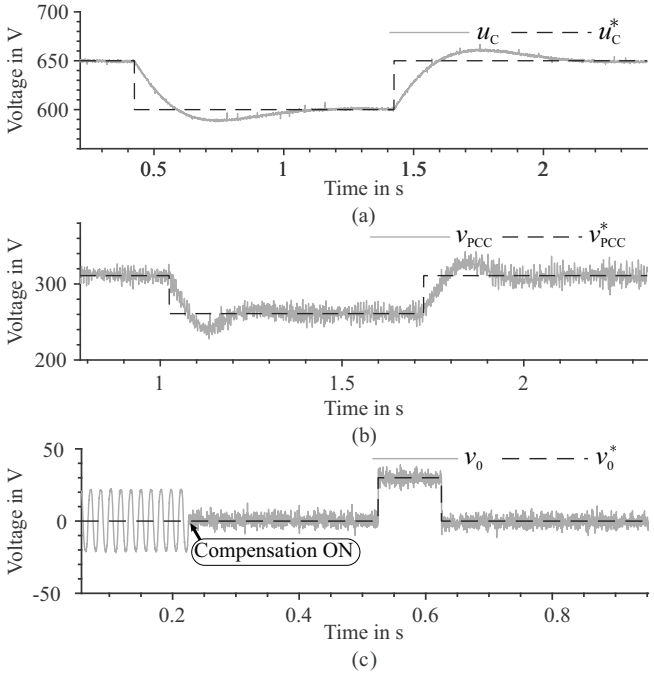

FIGURE 5. Experimental results for reference steps on the controlled voltages: (a) Dc bus. (b) PCC voltage. (c) PCC voltage on axis 0 from no-load to compensation on.

C. Analysis for three-phase nonlinear load

The connection of a three-phase nonlinear load to the microgeneration system introduces nonlinear characteristics in each phase of the system, with symmetrical magnitude and distribution due to the circuit characteristic. This results in harmonics that distort the voltage waveform. Although this load does not directly cause imbalances among phases, it can still impact compliance with power quality standards. In this context, an uncontrolled three-phase rectifier is connected to the PCC.

Figure 6 shows the harmonic content of the currents from the three-phase nonlinear load, as well as the power drawn by the load at the instant of its connection.

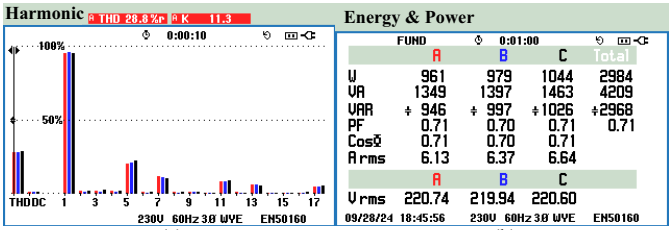

FIGURE 6. Content of the three-phase nonlinear load: (a) Harmonic content of the load current. (b) Power drawn by the load.

Figure 7 shows the reference tracking for the currents i_α, i_β and $i_{0,1}$ for a 4.2 kVA balanced nonlinear load. In this way, controllers present the ability to quickly trace the references imposed by the load on $i_\alpha{}^*$, $i_\beta{}^*$ and $i_{0,1}$. Reference $i_{0,1}$ remains null due to the characteristic of a balanced three-phase system without zero-sequence components.

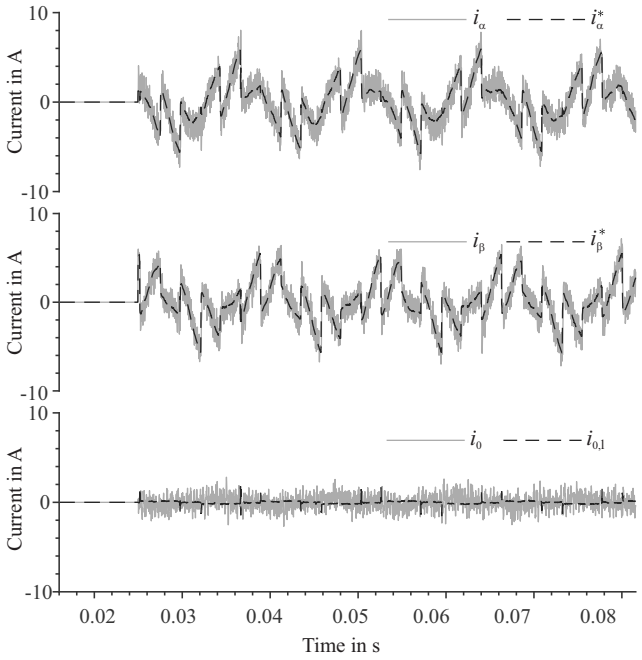

FIGURE 7. Results from DSP data for reference tracking in the αβ0 frame for a 4.2 kVA balanced three-phase nonlinear load.

Figure 8 shows the voltage waveform at the SEIG terminals (v_a, v_b and v_c), the PCC voltage (v_{PCC}), the load current ($i_{a,l}$, $i_{b,l}$ and $i_{c,l}$), the current processed by DSTATCOM (i_a, i_b and i_c). In this Figure, an adequate response for the regulation of the microgeneration system can still be observed, even with a nonlinear load.

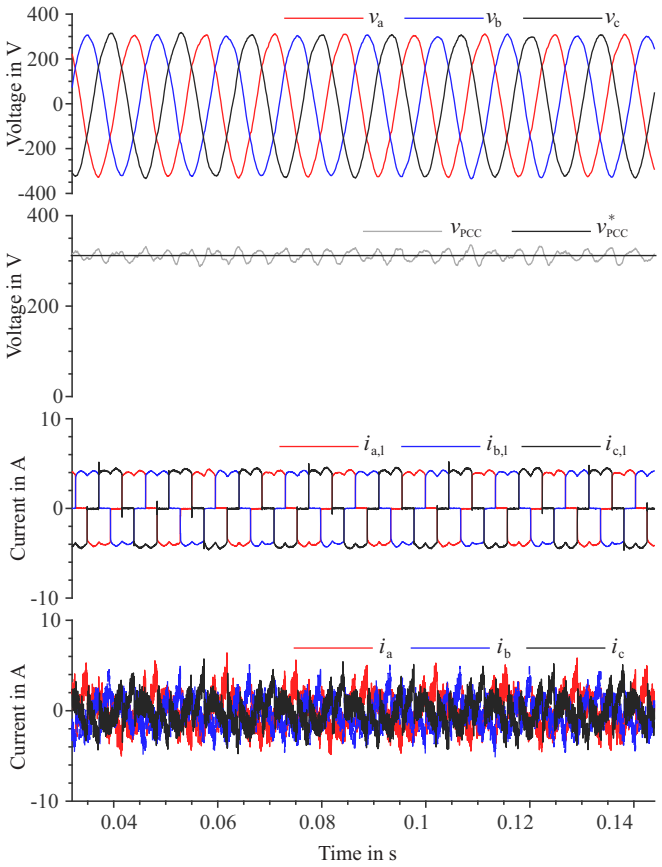

FIGURE 8. Steady-state behavior for 4.2 kVA load.

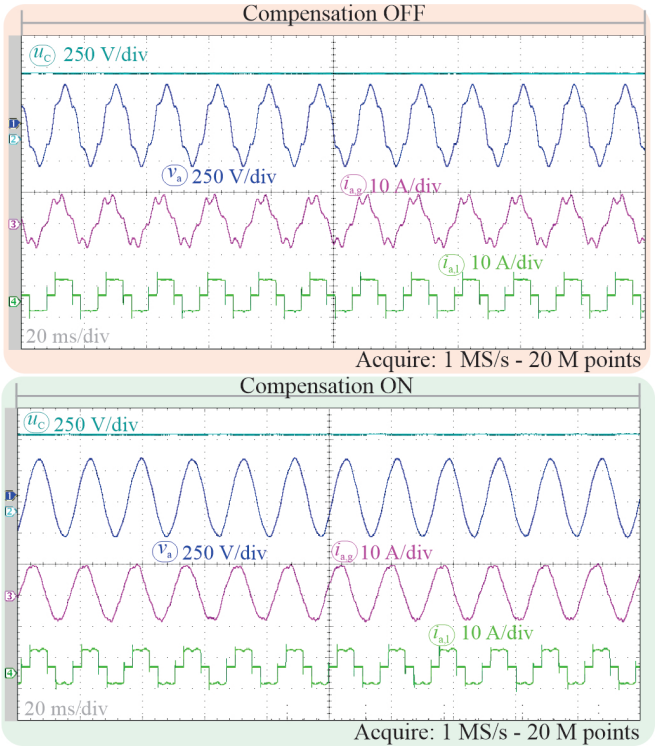

FIGURE 9. Steady-state behavior under 4.2 kVA three-phase nonlinear load: voltage and current waveforms, before and after compensation.

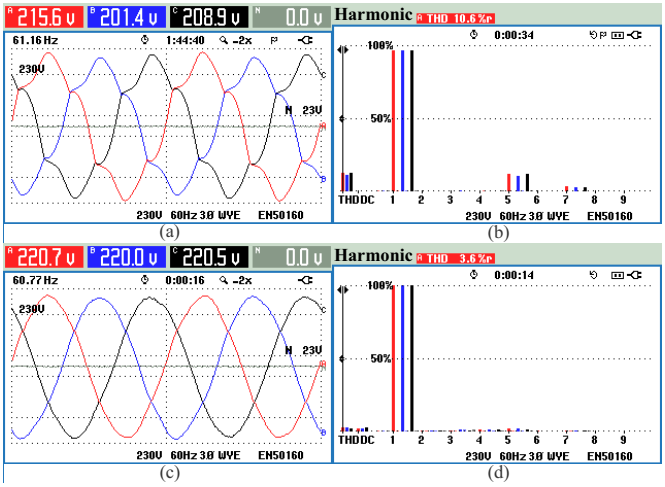

FIGURE 10. PCC voltages for three-phase balanced nonlinear load without compensation (4.2 kVA): (a) Uncompensated three-phase voltage waveforms. (b) Harmonic content without compensation. (c) Compensated three-phase voltage waveforms. (d) Harmonic content with compensation.

In the Figure 9, the waveform of the DC bus voltage of the VSI (u_C), the phase a voltage at the PCC (v_a), the phase a current of the SEIG ($i_{a,g}$), and the load current ($i_{a,l}$), were analyzed with and without compensation. It can be observed that with the control method, the microgeneration system provides adequate regulation even with a nonlinear load.

Figure 10 illustrates, from FLUKE 435, the voltage performance under the connection of a 4.2 kVA three-phase nonlinear load. Figure 10(a) shows the voltage sag without control. Figure 10(b) displays the harmonic content of the voltages without the designed control action, exceeding the limits set by the IEEE 519-2014 recommendations. In Figure 10(c), the PCC voltages are shown compensated by the control action performed by the DSTATCOM. Figure 10(d), analyzes the harmonic content of the steady-state voltage at the SEIG terminals. It also presents a reduction due to the compensating currents generated by the DSTATCOM, complying with the IEEE 519-2014 limits of 5% for individual harmonics and 8% for total harmonic distortion (THD).

D. Analysis for single-phase nonlinear loads

In the microgeneration system, connecting single-phase nonlinear loads subjects each phase to different current magnitudes and characteristics. This causes imbalances, generating not only harmonic distortions in the voltage waveforms but also introducing zero-sequence components, which compromise three-phase balance. The resulting unbalanced currents can flow through the neutral conductor, increasing losses and causing undesirable variations in system voltage levels. In this context, three single-phase uncontrolled rectifiers are sequentially connected to the PCC on phases a, b, and c, remaining simultaneously connected.

Figure 11 shows the harmonic content of the currents from the three nonlinear single-phase loads, as well as the power drawn by the load, respectively, highlighting the instant when both are simultaneously connected to the system.

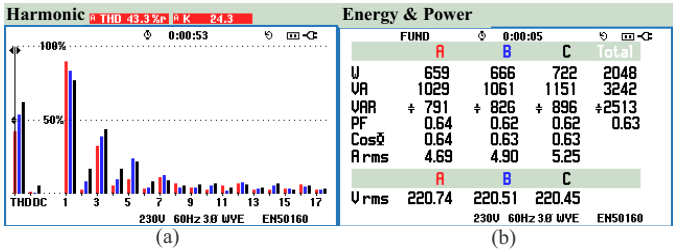

FIGURE 11. Content of the 1 kVA single-phase nonlinear loads: (a) Harmonic content of the load current. (b) Power drawn by the load.

Figure 12 shows the reference tracking for currents i_α, i_β, and i_0 for three 1 kVA single-phase nonlinear loads. These loads are uncontrolled single-phase rectifiers with different capacitor values, causing an imbalance among the system phases. The capacitor values in the 1 kVA single-phase rectifiers are 20 µF in the load connected to phase a, 15 µF in the load connected to phase b, and 100 µF in the load connected to phase c. The designed controllers demonstrate the ability to quickly track the references imposed by the loads on i_α^*, i_β^* and $i_{0,l}$. The reference $i_{0,l}$ represents the unbalanced current from the characteristics of a three-phase system with zero-sequence components. Even with the connection of three single-phase rectifiers with distinct capacitances, resulting in a high system imbalance, the response is adequate for voltage regulation.

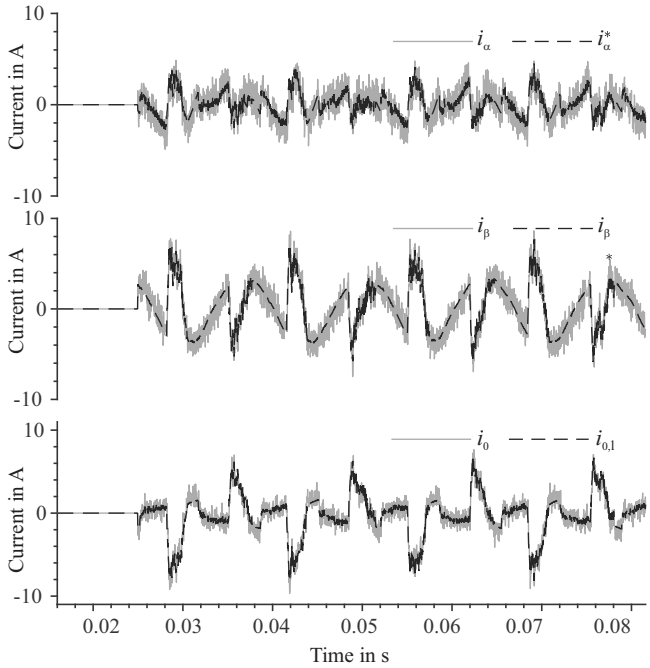

FIGURE 12. Results from DSP data for reference tracking in the αβ0 frame at 1 kVA for three different single-phase loads connected to each phase simultaneously.

Figure 13 shows the transient response of the system to the connection of the nonlinear single-phase loads. It is noted that the inverter currents mitigate the effects of distorted load currents, compensating for disturbances and maintaining voltage regulation at the PCC.

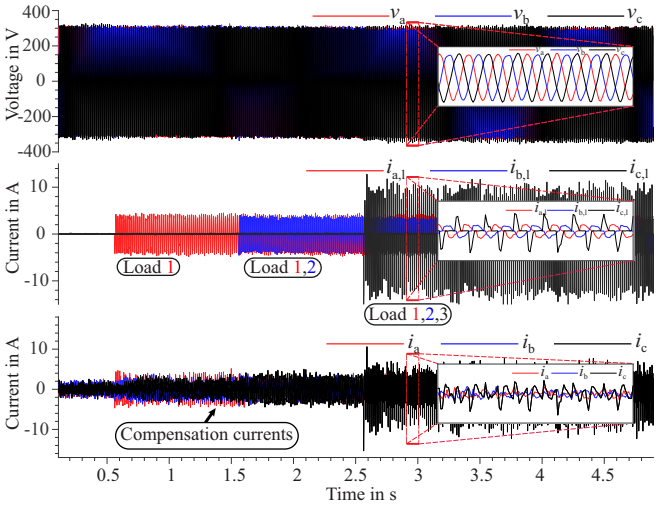

FIGURE 13. Connection transient of three single-phase loads (1 kVA rectifiers) connected to each phase (a, b, and c), respectively.

Figure 14 shows the voltage waveform at the SEIG terminals (v_a, v_b and v_c), The voltage (v_{PCC}), the load current ($i_{a,l}$, $i_{b,l}$ and $i_{c,l}$), the current processed by DSTATCOM (i_a, i_b and i_c). Even with the connection of three single-phase rectifiers with different capacitances, resulting in a high imbalance in the system, the response is adequate for voltage regulation.

Figure 15 shows the DC bus voltage of the VSI (u_C) and the zero-sequence voltage (v_0) during the connection of three uncontrolled single-phase rectifiers with different capacitances. These single-phase nonlinear loads naturally cause imbalances in the system, resulting in oscillations in the neutral wire voltage v_0. The quick response of the system to load transients is observed, maintaining zero voltage in the v_0 axis due to the performance of the OSV-MPC.

For Figure 16, the waveforms of the DC bus voltage of the VSI (u_C), the phase a voltage at the PCC (v_a), the phase a current of the SEIG ($i_{a,g}$), and current processed by the DSTATCOM in phase c, (i_c) were analyzed.

It was observed that the microgeneration system provided an adequate response for regulation, even with the connection of three unbalanced single-phase nonlinear loads.

In Figure 17, the compensation of imbalance by the DSTATCOM can be analyzed, resulting in balanced terminal voltages as shown in Figure 17(a). This meets the IEEE 1159-2009 standard for imbalance below 2% as illustrated in Figure 17(b) and also complies with the IEEE 519-2014 standard for voltage harmonics, as shown in Figures 17(c) and 17(d).

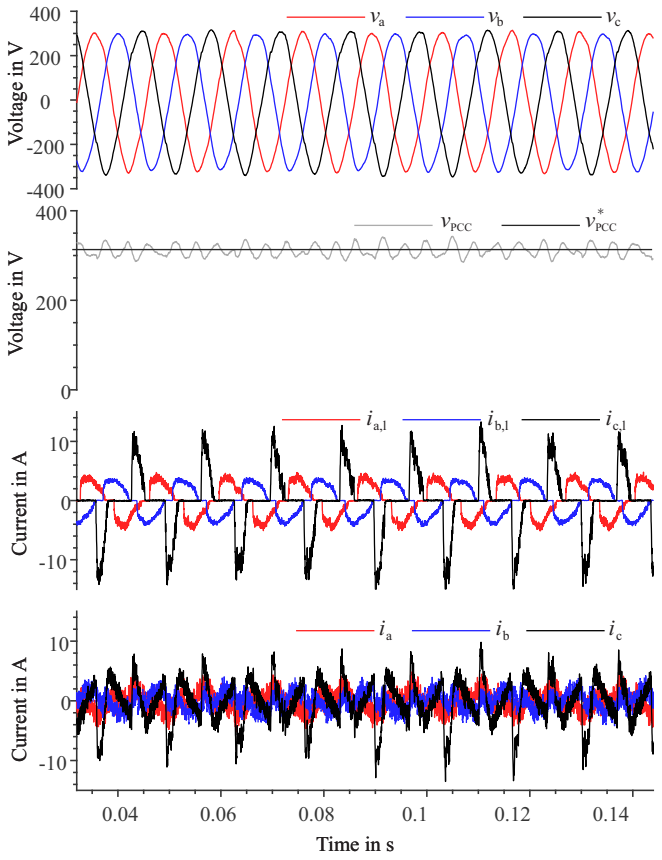

FIGURE 14. Results for three single-phase loads (rectifiers) of 1 kVA connected to each phase (a, b, and c).

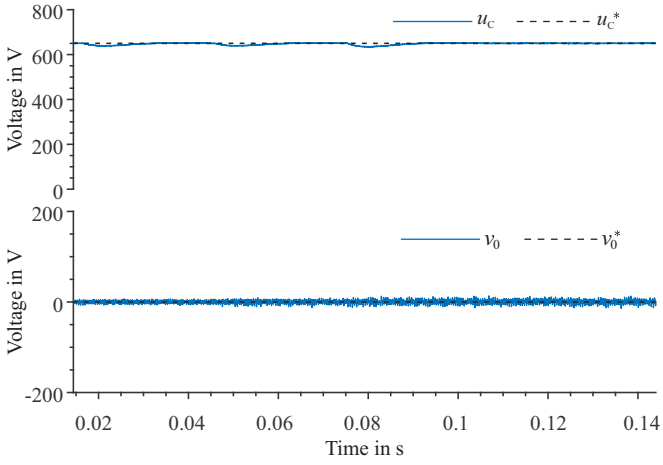

FIGURE 15. Transient response to connecting three 1 kVA nonlinear single-phase loads to phases (a, b, and c).

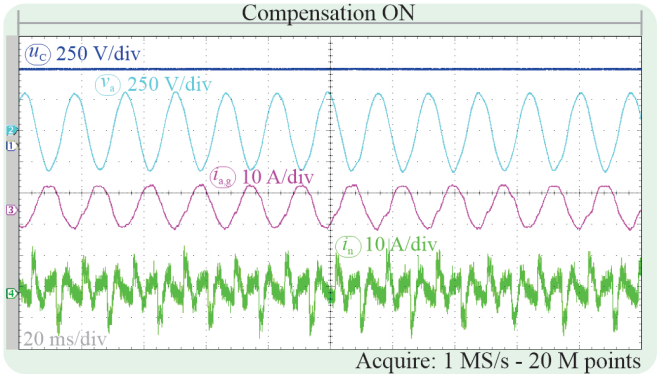

FIGURE 16. Steady-state behavior under single-phase nonlinear loads of 1 kVA connected to each phase (a, b, and c): voltage and current waveforms with compensation.

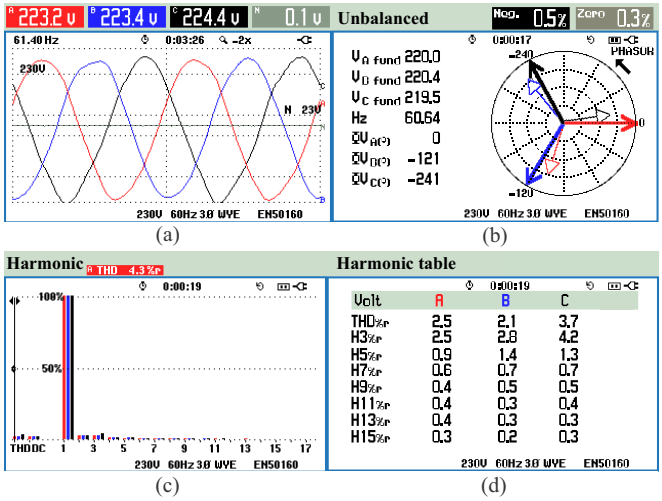

FIGURE 17. Steady-state behavior of PCC voltages (FLUKE 435) with compensation for three unbalanced single-phase nonlinear loads of 1 kVA: (a) Three-phase voltage waveforms. (b) PCC voltage imbalance. (c) Voltages harmonic content. (d) Harmonic content table.

V. CONCLUSION

This paper presented an OSV-MPC approach for voltage regulation at the PCC, along with imbalance regulation, in a four-wire SEIG-based off-grid microgeneration system. It also addressed harmonic and zero-sequence compensation. Experimental results validated the proposed method, demonstrating appropriate transient and steady-state responses. The THD analysis showed that the harmonic content in the PCC voltages met the IEEE 519-2014 standard recommendations. Furthermore, the voltage imbalance control drove the variables within the limits suggested by the IEEE 1159-2009 standard, representing a good performance even in a system with unregulated frequency. The design and implementation of the controller are straightforward and also require no hardware modifications. The proposed OSV-MPC strategy contributed to a better performance of the isolated microgeneration system presented.

ACKNOWLEDGMENT

This work was supported in part by the Coordenação de Aperfeiçoamento de Pessoal de Nível Superior - Brasil (CAPES/PROEX) - Finance Code 001, and in part by INCT-GD and its funding agencies (CNPq process nº 465640/2014-1, CAPES process nº 23038.000776/2017-54 and FAPERGS process nº 17/2551-0000517-1).

AUTHOR'S CONTRIBUTIONS

C. A. SOUZA: Conceptualization, Data Curation, Formal Analysis, Funding Acquisition, Investigation, Methodology, Project Administration, Resources, Software, Supervision, Validation, Visualization, Writing – Original Draft, Writing – Review & Editing. **G. M. COCCO:** Conceptualization, Data Curation, Formal Analysis, Funding Acquisition, Investigation, Methodology, Project Administration, Resources, Software, Supervision, Validation, Visualization, Writing – Original Draft, Writing – Review & Editing. **R. F. CAMARGO:** Conceptualization, Formal Analysis, Investigation, Methodology, Software, Supervision, Validation, Visualization, Writing – Original Draft, Writing – Review & Editing. **F. E. BISOGNO:** Conceptualization, Methodology, Resources, Visualization. **M. WOLTER:** Conceptualization, Formal Analysis, Investigation, Project Administration, Resources, Supervision.

PLAGIARISM POLICY

This article was submitted to the similarity system provided by Crossref and powered by iThenticate – Similarity Check.

REFERENCES

[1] U. K. Kalla, B. Singh, P. Kumar, K. L. Agarwal, S. Murthy, "State-of-the-art and comprehensive study of renewable energy sources based microgrid with single-phase self-excited induction generator", *IET Renewable Power Generation*, vol. 14, no. 18, pp. 3699–3714, 2020, doi:10.1049/iet-rpg.2020.0800.

[2] A. S. Lunardi, A. J. Sguarezi Filho, "Controle preditivo baseado em modelo para sistema eólico empregando gerador de indução gaiola de esquilo", *Eletrônica de Potência*, vol. 23, no. 3, pp. 330–338, 2018, doi:10.18618/REP.2018.3.2788.

[3] S. Kewat, B. Singh, I. Hussain, "Power management in PV-battery-hydro based standalone microgrid", *IET Renewable Power Generation*, vol. 12, no. 4, pp. 391–398, 2017, doi:10.1049/iet-rpg.2017.0566.

[4] Y. K. Chauhan, S. K. Jain, B. Singh, "A Prospective on Voltage Regulation of Self-Excited Induction Generators for Industry Applications", *IEEE Transactions on Industry Applications*, vol. 46, no. 2, pp. 720–730, March 2010, doi:10.1109/TIA.2009.2039984.

[5] C. B. Tischer, L. G. Scherer, R. F. de Camargo, "Topologia Híbrida Trifásica a Três Fios para Regulação de Tensão em Sistemas de Geração Baseados em Gerador de Indução Auto-excitado", *Eletrônica de Potência*, vol. 20, no. 1, pp. 40–49, 2015, doi:10.18618/REP.2015.1.040049.

[6] L. G. Scherer, R. V. Tambara, R. F. de Camargo, "Voltage and frequency regulation of standalone self-excited induction generator for micro-hydro power generation using discrete-time adaptive control", *IET Renewable Power Generation*, vol. 10, no. 4, pp. 531–540, 2016, doi:10.1049/iet-rpg.2015.0321.

[7] G. M. Cocco, J. d. A. Borges, M. Stefanello, F. B. Grigoletto, "Finite Set Model Predictive Control of Four-Leg Split-Source Inverters", *in 2018 13th IEEE International Conference on Industry Applications (INDUSCON)*, pp. 630–635, Nov 2018, doi:10.1109/INDUSCON.2018.8627303.

[8] C. A. Souza, G. M. Cocco, R. F. De Camargo, M. L. Flach, F. E. Bisogno, "FS-MPC Approach for Zero-Sequence Compensation in SEIG-Based Off-Grid Systems", *in 2023 IEEE 8th Southern Power Electronics Conference and 17th Brazilian Power Electronics Conference (SPEC/COBEP)*, pp. 1–6, 2023, doi:10.1109/SPEC56436.2023.10408081.

[9] S. Kouro, P. Cortés, R. Vargas, U. Ammann, J. Rodríguez, "Model predictive control—A simple and powerful method to control power converters", *IEEE Transactions on Industrial Electronics*, vol. 56, no. 6, pp. 1826–1838, 2009, doi:10.1109/TIE.2008.2008349.

[10] S. Vazquez, J. Rodriguez, M. Rivera, L. G. Franquelo, M. Norambuena, "Model Predictive Control for Power Converters and Drives: Advances and Trends", *IEEE Trans on Ind Electron*, vol. 64, no. 2, pp. 935–947, Feb 2017, doi:10.1109/TIE.2016.2625238.

[11] M. Rivera, V. Yaramasu, J. Rodriguez, B. Wu, "Model Predictive Current Control of Two-Level Four-Leg Inverters-Part II: Experimental Implementation and Validation", *IEEE Transactions on Power Electronics*, vol. 28, no. 7, pp. 3469–3478, July 2013, doi:10.1109/TPEL.2012.2227825.

[12] L. G. Scherer, C. B. Tischer, R. F. de Camargo, "Voltage regulation of stand-alone micro-generation SEIG based system under nonlinear and unbalanced load", *in 2015 IEEE 24th International Symposium on Industrial Electronics (ISIE)*, pp. 428–433, 2015, doi:10.1109/ISIE.2015.7281506.

[13] C. B. Tischer, J. R. Tibola, L. G. Scherer, R. F. de Camargo, "Proportional-resonant control applied on voltage regulation of standalone SEIG for micro-hydro power generation", *IET Renewable Power Generation*, vol. 11, no. 5, pp. 593–602, 2017, doi:10.1049/iet-rpg.2016.0857.

[14] G. Attuati, R. F. de Camargo, L. G. Scherer, "Proportional-Resonant Stator Current Controller Applied to SEIG Based Systems", *in 2019 IEEE PES Innovative Smart Grid Technologies Conference - Latin America (ISGT Latin America)*, pp. 1–6, 2019, doi:10.1109/ISGT-LA.2019.8895502.

[15] G. M. Cocco, L. G. Scherer, F. B. Grigoletto, R. F. de Camargo, "Proportional-Resonant Controller Applied to DSTATCOM in a Hybrid Hydro-PV Generation System", *in Congresso Brasileiro de Automática-CBA*, vol. 2, 2020, doi:10.48011/asba.v2i1.1608.

[16] C. A. de Souza, G. M. Cocco, L. G. Scherer, R. F. de Camargo, "Proportional Integral Resonant and Proportional Derivative Controllers Applied to Zero Sequence Harmonic Compensation in Four-Wire Microgeneration Systems", *Journal of Control, Automation and Electrical Systems*, vol. 34, no. 2, pp. 443–454, 2023, doi:10.1007/s40313-022-00973-4.

[17] J. Rodriguez, M. P. Kazmierkowski, J. R. Espinoza, P. Zanchetta, H. Abu-Rub, H. A. Young, C. A. Rojas, "State of the Art of Finite Control Set Model Predictive Control in Power Electronics", *IEEE Transactions on Industrial Informatics*, vol. 9, no. 2, pp. 1003–1016, 2013, doi:10.1109/TII.2012.2221469.

[18] M. G. Judewicz, S. A. González, N. I. Echeverría, J. R. Fischer, D. O. Carrica, "Generalized Predictive Current Control (GPCC) for Grid-Tie Three-Phase Inverters", *IEEE Transactions on Industrial Electronics*, vol. 63, no. 7, pp. 4475–4484, 2016, doi:10.1109/TIE.2015.2508934.

[19] L. M. A. Caseiro, A. M. S. Mendes, S. M. A. Cruz, "Dynamically Weighted Optimal Switching Vector Model Predictive Control of Power Converters", *IEEE Transactions on Industrial Electronics*, vol. 66, no. 2, pp. 1235–1245, 2019, doi:10.1109/TIE.2018.2829689.

[20] P. Cortes, J. Rodriguez, C. Silva, A. Flores, "Delay Compensation in Model Predictive Current Control of a Three-Phase Inverter", *IEEE Trans on Ind Electron*, vol. 59, no. 2, pp. 1323–1325, 2012, doi:10.1109/TIE.2011.2157284.

[21] H. Akagi, E. H. Watanabe, M. Aredes, *Instantaneous Power Theory and Applications to Power Conditioning*, Wiley, 2017, doi:10.1002/9781119307181.

[22] S. Kwak, S.-J. Yoo, J. Park, "Finite control set predictive control based on Lyapunov function for three-phase voltage source inverters", *IET Power Electronics*, vol. 7, no. 11, pp. 2726–2732, 2014, doi:10.1049/iet-pel.2014.0044.

[23] M.-D. Ngo, V.-Q.-B. Ngo, K. A. Nguyen, D.-H. Le, H. Tran, "A powerful model predictive control via stability condition for direct matrix converter", *SN Applied Sciences*, vol. 2, no. 12, p. 2019, 2020, doi:10.1007/s42452-020-03857-x.

[24] V.-T. Le, H.-H. Lee, "Robust finite-control-set model predictive control for voltage source inverters against LC-filter parameter mismatch and variation", *Journal of Power Electronics*, vol. 22, no. 3, pp. 406–419, 2022, doi:10.1007/s43236-021-00379-6.

[25] P. Cortes, S. Kouro, B. La Rocca, R. Vargas, J. Rodriguez, J. I. Leon, S. Vazquez, L. G. Franquelo, "Guidelines for weighting factors design in Model Predictive Control of power converters and drives", *in 2009 IEEE International Conference on Industrial Technology*, pp. 1–7, 2009, doi:10.1109/ICIT.2009.4939742.

[26] O. Machado, P. Martín, F. J. Rodríguez, E. J. Bueno, "A Neural Network-Based Dynamic Cost Function for the Implementation of a Predictive Current Controller", *IEEE Transactions on Industrial Informatics*, vol. 13, no. 6, pp. 2946–2955, 2017, doi:10.1109/TII.2017.2691461.

[27] S. Vazquez, E. Zafra, R. P. Aguilera, T. Geyer, J. I. Leon, L. G. Franquelo, "Prediction Model With Harmonic Load Current Components for FCS-MPC of an Uninterruptible Power Supply", *IEEE Transactions on Power Electronics*, vol. 37, no. 1, pp. 322–331, 2022, doi:10.1109/TPEL.2021.3098948.

BIOGRAPHIES

Carlos Antônio de Souza, received his B.Sc. degree (2016) in Electrical Engineering from the Integrated Regional University of Alto Uruguai and Missões (URI), Brazil, and the M.Sc. degree (2019) from the Federal University of Santa Maria (UFSM), Brazil. Currently, he is working towards a Ph.D. degree at UFSM with the Power Electronics and Control Research Group (GEPOC). His research interests include microgeneration systems and applied control.

Gabriel Maier Cocco received his B.Sc. degree in Electrical Engineering from the Federal University of Pampa, Brazil, in 2018, and his M.Sc. degree from the Federal University of Santa Maria (UFSM), Brazil, in 2021. He is currently a Ph.D. candidate with co-supervision at UFSM and Otto-von-Guericke University Magdeburg, Germany. His research interests include renewable power generation and conditioning, as well as modeling and control of power converters.

Robinson Figueiredo de Camargo received his B.Sc. (2000), M.Sc. (2002), and Ph.D. (2006) degrees in Electrical Engineering from the Federal University of Santa Maria (UFSM), Brazil. He was the Coordinator of the Undergraduate Program in Control and Automation Engineering at UFSM from 2010 to 2012. Currently, he is head of the Department of Electric Power Processing at UFSM. His areas of interest include renewable energy sources, synchronization methods, power quality, DSTATCOM, and active power filters.

Fábio Ecke Bisogno received his B.Sc. (1999) and M.Sc. degrees in Electrical Engineering from the Federal University of Santa Maria (UFSM), Brazil, in 2001, and the Ph.D. degree in Electrical Engineering from Technische Universität Chemnitz, Germany, in 2006. He worked at the Fraunhofer Institute from 2003 to 2009. From 2009 to 2023, he worked as a Professor with UFSM. Currently, he is a Professor with the Koblenz University of Applied Sciences, Germany. His areas of interest are resonant converters, self-oscillating electronic converters, artificial lighting, and uninterruptible power supply.

Martin Wolter received his diploma in Electrical Engineering in 2006, his Dr.-Ing degree in 2008, and his venia legendi in 2012, all from Leibniz University Hannover, Germany. From 2011 to 2015, he worked at 50Hertz Transmission GmbH in system operation concept development. Since 2015, he has been the head of the Chair of Electric Networks and Renewable Energy at Otto-von-Guericke University Magdeburg, Germany. His research topics are power system modeling and simulation, system security and system operation, as well as power system dynamics.